Article

Photophysical Properties of Donor−Acceptor−π Bridge−Acceptor Sensitizers with a Naphthobisthiadiazole Auxiliary Acceptor: Toward Longer-Wavelength Access in Dye-Sensitized Solar Cells

Juganta K. Roy, Ravinder Kaur, Andrew Daniel, Alexandra Baumann, Qing Li, Jared H. Delcamp,* and Jerzy Leszczynski*
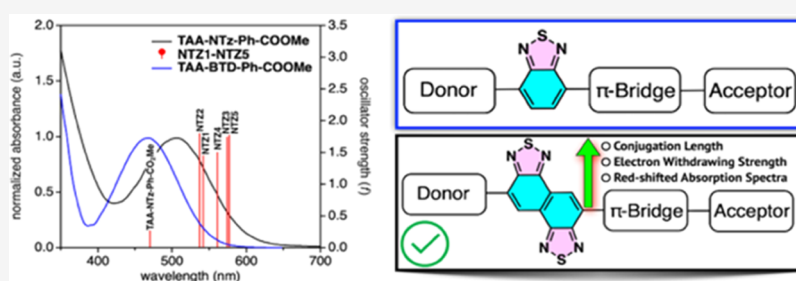
ACCESS | Metrics & More | Article Recommendations | SI Supporting Information

ABSTRACT: Accessing longer-wavelength photons is a critical research direction in dye-sensitized solar cells (DSSCs). Currently, dye-sensitized solar cells are exceptional at generating high photovoltages with shorter wavelength photons, but few examples exist of DSSCs using photons in the shortwave infrared region (>1000 nm). New dye building blocks are critical toward accessing these longer-wavelength photons. With this in mind, five new triphenylamine-based metal-free dyes derived from a donor−auxiliary acceptor−π bridge−acceptor (D−A′−π−A) structure are characterized theoretically for application in dye-sensitized solar cells (DSSCs). The driving force of electron injection, the spontaneity of dye regeneration, charge-transfer length, and partial density of states of the isolated and TiO$_2$-bound dyes, which are all critical to DSSC performance, are systematically investigated via first-principles calculations. We find that replacing the high-performing benzothiadiazole (BTD) auxiliary acceptor building block with a longer conjugation length and stronger electron-withdrawing building block, naphtho[1,2-c:5,6-c′]bis([1,2,5]thiadiazole) (NTz), is beneficial toward the kinetics of charge injection along with reducing the optical energy gap of the designed dyes. The obtained results imply that using the NTz unit extends the absorption spectrum toward longer wavelengths and improves charge separation due to the planarity and conjugation length extension that arises from the NTz fragment. The shift of the conduction band of TiO$_2$ (ΔE_{CB} value) is higher for the designed NTz-based dyes than for the BTD-based dye on TiO$_2$, suggesting that the open-circuit voltage (V_{OC}) of a dye-sensitized solar cell device will also be higher. Concerning the photophysical properties of the dyes, the NTz-based dyes are promising as they possess a longer excited state and longer radiative lifetime than a BTD-based dye. We synthesize a model NTz-based dye and a BTD analogue for comparison with computational results. The optical properties of the NTz-based dye are computed to validate our computational approach, which agrees with the experimental observations. Our combined computational and experimental approach sheds light on the physical principle of molecular photogenerated charge transfer and provides valuable guidance for the further molecular synthesis of long-wavelength absorbing materials.

■ INTRODUCTION

Accessing green energy is a frontier concern in fundamental and industrial research since greenhouse gases originate from the combustion of fossil fuels depleting the ozone layer.[1−3] Renewable energy, such as solar energy,[4,5] represents one of the most efficient and cheapest routes to access a renewable energy source. Over the last two decades, photovoltaics such as dye-sensitized solar cells (DSSCs) introduced by O'Regan and Grätzel[6] in 1991 have gained considerable interest as an alternative renewable energy source.[7−13] Currently, DSSCs have shown the highest performance of any solar cell technology in low-photon flux situations (e.g., indoor lighting,

tandem solar cells, underwater applications), are an affordable solar cell technology, and have shown some of the highest photovoltages observed among solar cells in the short-wavelength visible region.[14] However, DSSCs can be further improved by enhancing long-wavelength light absorption. DSSC devices rarely utilize photons past ~900 nm despite a large portion of the solar spectrum existing beyond 900 nm.[15] This shortcoming limits their performance in full sun intensity
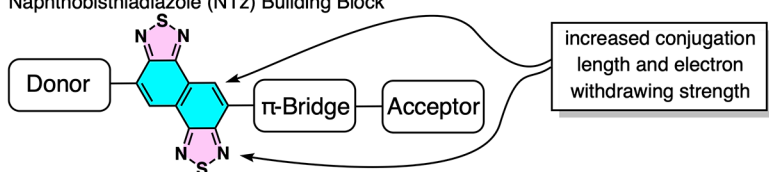
A

Prior Work:
Common Benzothiadiazole (BTD) Building Block
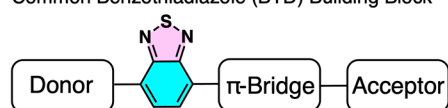
This Work:
Naphthobisthiadiazole (NTz) Building Block

increased conjugation length and electron withdrawing strength

Notable High Performing Dyes with BTD Building Blocks

XW61
used in a 12.4% PCE iodide redox shuttle based device

SGT-021
co-sensitizer in a 14.2% PCE sunlight converting device

XY1b
co-sensitizer in a 34.5% PCE fluorescent light converting DSSC

ZL003
sensitizer in a 13.6% PCE sunlight converting device
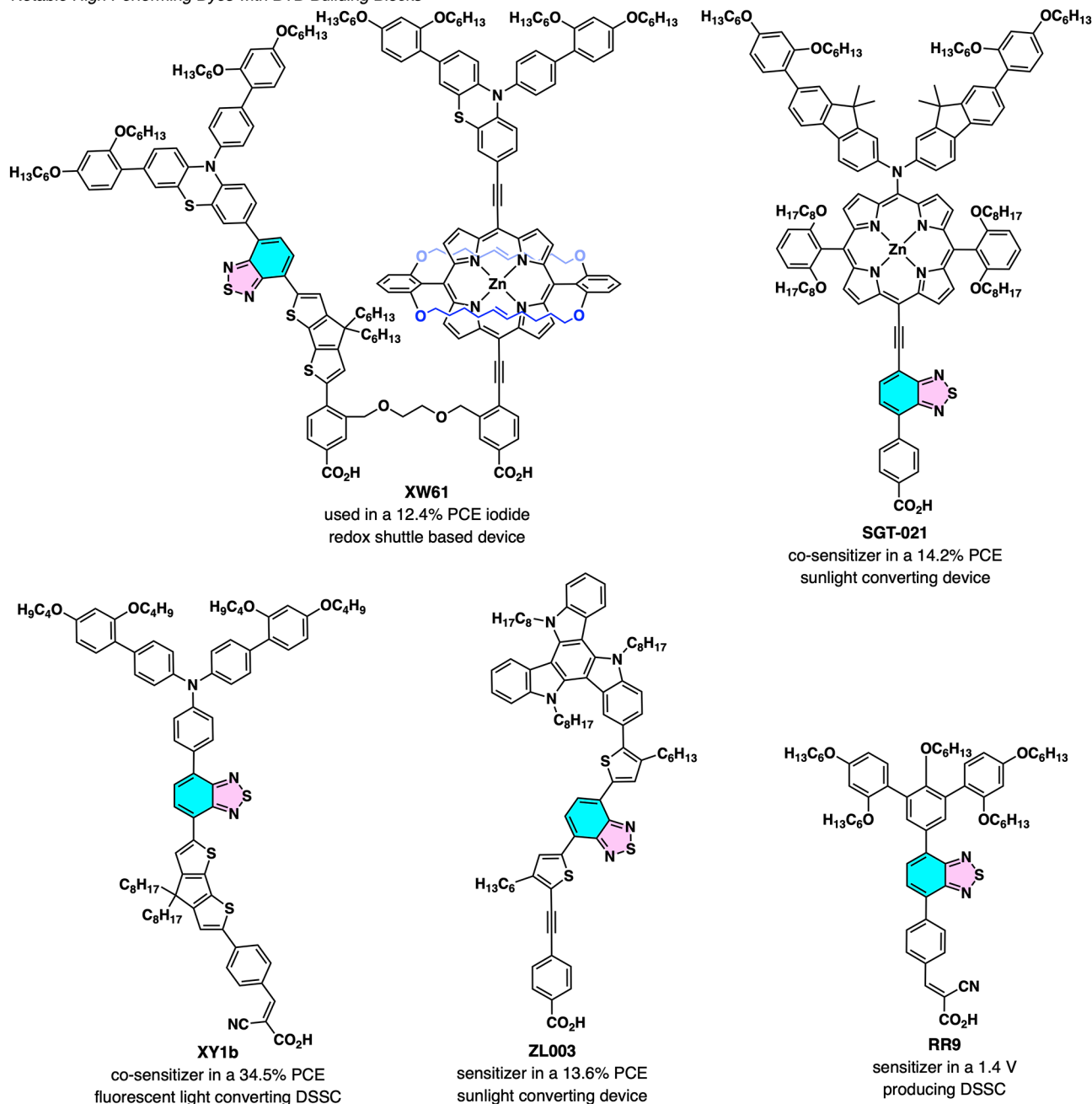
RR9
sensitizer in a 1.4 V producing DSSC

Figure 1. Comparison of BTD and NTz building blocks with the conjugation path highlighted in the blue rings and the withdrawing thiadiazole groups highlighted in the purple rings. High-performing DSSC dyes are shown with the BTD building block highlighted in each.

and outdoor low light situations. Since the sensitizer in these systems is responsible for the photon absorption step, the discovery of a sensitizer that can absorb long-wavelength photons (>900 nm) and convert these photons into electricity inside a DSSC device is critically important to improving

DSSC performance. A key limitation to designing such a sensitizer is the limited building block selection with which current photosensitizers are made. Thus, the discovery of building blocks that red-shift the absorption spectrum of DSSC dyes without harming the rate of key electron-transfer
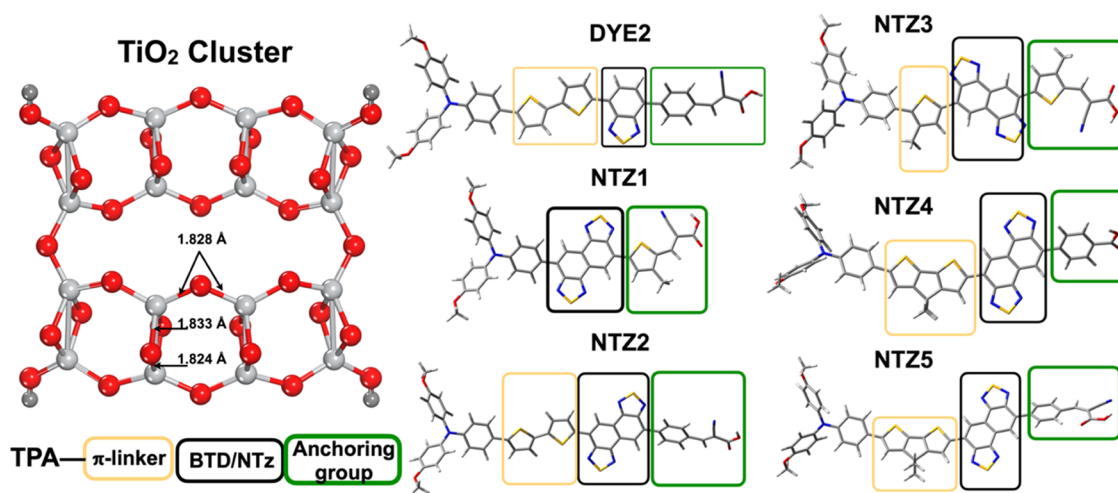
Figure 2. Optimized $(TiO_2)_{16}$ cluster, structures of the proposed NTz-based (**NTZ**) dye molecules and reference dye (**DYE2**). Different color boxes indicate the substituting of corresponding fragments in the **DYE2** structure. Longer hexyl chains are not considered in the calculations. Yellow, black, and green boxes represent the π-linker, auxiliary acceptor (BTD or NTz), and π-spacer-anchoring groups, respectively.

processes within the DSSC device is crucial to discovering high-performance long-wavelength absorbing sensitizers.

The conventional DSSC device consists of a sensitizer, electrolyte, a photoanode, and a photocathode, where the sensitizer plays the most critical role in harvesting photons and thus governs the power conversion efficiency (PCE) of the device. The conversion of photons to electricity in DSSC devices depends on four basic steps: (1) the sensitizer reaching an excited state after the absorption of photons from sunlight, (2) the photoexcited sensitizer injecting electrons into the conduction band (CB) of a semiconductor such as TiO_2, (3) the oxidized sensitizer being regenerated by accepting electrons from an electrolyte such as one containing iodide, and (4) the electrolyte being reduced at a counter electrode such as platinum. The excitation, injection, and regeneration steps are all dramatically influenced by the sensitizer, and the iterative design of sensitizers has led to the highest-performing DSSC devices to date by controlling these steps. Currently, the excitation step can be substantially improved upon since a large amount of the solar spectrum is not used in DSSCs because of limited dye absorption ranges. Dyes with broader absorption that retain high quantum efficiency with respect to the injection and regeneration steps are urgently needed to progress the DSSC field further.

The tunable nature of sensitizers in DSSCs has created a significant push in research efforts to design efficient sensitizers. The donor$-\pi$ bridge$-$acceptor (D$-\pi-$A) framework represents a push$-$pull system that is responsible for good intramolecular charge-transfer (ICT) events and charge separation upon photoexcitation.[16,17] Each of these three building blocks (the donor, π-bridge, and acceptor) is readily interchanged allowing for a substantial number of possible dye permutations. Additionally, a modification to the D$-\pi-$A framework was introduced by Zhu et al.,[18] which incorporates an auxiliary acceptor (A′) in between D and π, which creates a D$-$A′$-\pi-$A framework. This design requires that the A′ group has good electronic communication from the donor to the π-bridge for strong photon absorption, which is unique when compared to the acceptor group of the D$-\pi-$A design that is only required to electronically communicate well with the π-bridge. The DSSC community has examined significant

permutations with the D$-\pi-$A and D$-$A′$-\pi-$A approaches resulting in higher PCE DSSCs.[5,19−23]

Dramatic improvements to DSSCs are possible by introducing new A′-type building blocks that allow for the construction of dyes absorbing at longer wavelengths. Low-energy gap dye-generating conjugated electron-withdrawing units are beneficial to tailor molecular structures, modulate the energy levels, shift absorption spectra, and improve the photostability of sensitizers. In 2012, Haid et al. reported that inserting an additional phenyl ring between the benzothiadiazole (BTD) and the cyanoacrylic acid (CA) significantly improves the PCE by ∼6.5 times, whereas charge recombination of electrons in TiO_2 with the oxidized dye slows the back electron transfer down by up to 5 times.[24] The sensitizer consists of a triarylamine (TAA)-bithiophene donor, BTD as an auxiliary acceptor, benzene as π-spacer, and CA as an acceptor/anchoring group (coded **DYE2** here, see Figure 1 for general BTD information and Figure 2 for the specific dye structure). Importantly, the BTD building block[25,26] has been used in nearly all of the highest efficiency and highest photovoltage generating DSSC devices (Figure 1).[27−33] However, A′-type building blocks that enable longer-wavelength absorption are needed to improve further substantially. The limited conjugation length and withdrawing strength of the BTD building block are design elements that can be significantly improved upon. Recently, the electron-withdrawing units of benzotriazole,[34,35] thienopyrazine,[36] thieno-thiophene,[37] quinoxaline,[38,39] diketopyrrolopyrrole,[40,41] and naphtho[1,2-c:5,6-c']bis[1,2,5]thiadiazole (NTz)[42] have been examined as auxiliary acceptor-type building blocks for sensitizers in DSSCs.

Higashino et al.[42] reported that the NTz unit shifts the absorption and emission spectrum into the NIR region of porphyrin dyes and functions as an efficient electron acceptor in DSSCs. The NTz building block extends the conjugation of the BTD building block, and the NTz building block is stronger withdrawing with two thiadiazole groups (Figure 1). Since both of these properties are important properties to incorporate in future dye designs, we sought to explore the NTz unit in nonporphyrin organic dyes with a strong ICT character. NTz fragments are well known for applications in polymer solar cells with higher electron-accepting ability than

BTD groups.[43−45] Additionally, the NTz unit is a rigid unit that can incorporate planarity while extending conjugation in the molecule to enhance ICT. Based on this observation, we have designed five different dyes by substituting the BTD unit with the NTz unit. Additional modifications to the TAA−π-linker moiety, π-spacer, and anchoring group have been evaluated. We have implemented a comprehensive quantum chemical protocol to investigate photophysical properties and charge-transfer phenomena at the dye/semiconductor interface of the designed dyes and reference dye. Finally, we have synthesized a model organic NTZ dye, inspired by the results of the computational studies.

Computational Details. To explore the photophysical properties of NTz-based dyes, we have implemented density functional theory (DFT)/time-dependent (TD)-DFT approaches via the Gaussian 09 program.[46] Five NTz-based dyes, designed by substituting the BTD unit of **DYE2** with NTz, are depicted in Figure 2. Ground- and excited-state optimizations are performed using the PBE0[47] hybrid functional and the Coulomb attenuating ωB97XD functional[48] for the isolated dyes and dye/TiO$_2$ clusters, respectively. In both cases, the 6-311G(d,p) basis set for C, N, O, and S atoms was used, while effective core potential (ECP) LANL2DZ and its corresponding basis set were applied for Ti atoms. The ωB97XD functional including long-range correction was chosen to calculate the vertical excitation energies and the oscillator strengths within the TD-DFT framework with the above-mentioned basis sets. ωB97XD is considered one of the best methods to predict reasonable excitation energies correlated to the absorption spectra of charge-transfer dyes.[49,50] The choice of functional and benchmarking is discussed in the Supporting Information. To match experimental observations, the ω parameter is tuned, and the method is termed OT-ωB97XD (see the Supporting Information) in this article unless otherwise mentioned. Harmonic vibrational frequencies were computed to confirm that all stationary points on the potential energy surface represent minimum energy structures. We have incorporated solvent effects at both the DFT and TD-DFT levels of theory using a conductor-like polarizable continuum (C-PCM) model[51] with dichloromethane (DCM) solvent (ε: 8.93) as is used during the characterization of **DYE2**. The TD-DFT single-point calculations were performed with the solvent-phase DFT-optimized geometry. The lowest 10 singlet−singlet transitions of the optimized ground-state geometry in the gas and solvent phase were selected to obtain vertical excitation energies and oscillator strengths of the dyes and dye−TiO$_2$ complexes. We also have optimized the first excited state of all of the dyes using the same level of theory.

A dye can be bound to the TiO$_2$ cluster by three modes: monodentate, chelated, and bridged bidentate, where the latter mode is widely accepted in DSSC research.[52−54] The $[(TiO_2)_{16}(H_2O)_2]$ cluster is used to simulate the anatase TiO$_2$(101) surface. This cluster model has been successfully studied for the adsorption of different dyes in our previous studies.[11] Persson et al.[55] explained that small-scale theoretical models of TiO$_2$ give acceptable results without showing significant discrepancies compared to large models.[9,56] Small clusters like (TiO$_2$)$_{16}$ usually provide rational outcomes in small-scale theoretical models and exhibit insignificant variances with large and periodic models.[9,57−60] The optimized (TiO$_2$)$_{16}$ cluster with the important bond lengths is depicted in Figure 2. Electron excitation analysis and hole−electron-
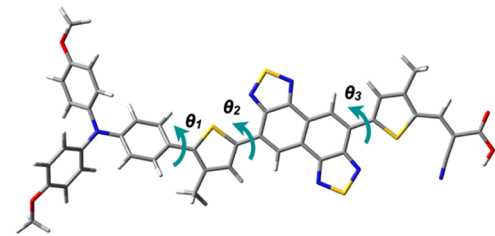
related indices were computed using the Multiwfn package.[61,62] Due to computational cost, −OC$_6$H$_{13}$ groups in the experimental species were replaced by −OCH$_3$ in our model compound, as longer alkyl chains predominantly do not affect the absorption properties. Natural population analysis[63] (NPA) based on the PBE0 density matrix has been carried out to confirm the charge transfer from the dye to the TiO$_2$ surface.

■ RESULTS AND DISCUSSION

We have designed five dyes based on the reported species (**DYE2**) by Haid et al.[24] We have modified the known dye by systematically changing the auxiliary acceptor and anchoring groups from cyanoacrylic acid to benzoic acid. DFT and TD-DFT computations were implemented to evaluate the newly designed dyes to gain insight into the electron injection and back electron-transfer reactions at the dye−semiconductor interface.

Geometrical Structure. Five NTZ-based D−A′−π−A dyes are designed and evaluated by DFT/TD-DFT approaches with and without a π-linker between the D and A′ units. Here, we consider triphenylamine derivatives as donors, thiophene or CPDT derivatives as π-linkers, naphtho[1,2-c:5,6-c′]bis-({1,2,5}thiadiazole) (NTz) as an auxiliary acceptor (A′), and two anchoring units such as cyanoacrylic acid (CA) and benzoic acid (BA). The degree of coplanarity governs the absorption spectra and charge-transfer properties in organic dyes. Different dihedral angles of the ground-state-optimized geometries were computed and are tabulated in Table 1. The

Table 1. Different Dihedral Angles of NTZ Dyes and DYE2 Computed at the DFT/PBE0/6-311G(d,p) Level of Theory with Structures Optimized in Dichloromethane Solvent

dihedral angle	NTZ1	NTZ2	NTZ3	NTZ4	NTZ5	DYE2
θ_1	31.76	22.41	37.46	22.05	22.18	24.53
θ_2		2.65	8.18	3.70	2.22	6.18
θ_3	1.32	34.91	2.67	37.25	35.62	32.92

dihedral angle (θ_1) between the TAA and π-spacer is higher in the **NTZ3** dye due to increased steric with the alkyl thiophene π-linker. θ_1 is lower for the **NTZ2** dye, which differs from the reference dye only at the BTD to NTz change. It is noted that the **NTZ1** dye is without a π-linker between the D and A′ units; hence, the dihedral angle definition differs from the other dyes. Dihedral angle (θ_2) is higher for the alkyl thiophene π-linker between the D and A′ units than the remaining dyes, which possess only small deviations in θ_2. However, dihedral angle (θ_3) largely deviates based on the ring size, e.g., a five-membered ring shows small angles, while six-membered rings induce an out-of-plane torsion of ∼35^0 with respect to the A′ unit. All of the dyes have reasonable dihedral angles for application in DSSC devices with reduced dihedral angles in many cases relative to the reference dye.

Energetics of Isolated and TiO$_2$ Bounded Dyes. The frontier molecular orbitals (FMOs) are crucial in providing information about the photoexcitation properties of chromophores like organic molecules.[64] A detailed description of FMOs is needed to get insight into the charge-transfer behavior of the dyes used in solar cells. The energy gap between the FMOs, namely, the highest occupied molecular orbital (HOMO) and lowest unoccupied molecular orbital (LUMO), is known as the optical energy gap (E_{gap}^{opt}), which determines the photon conversion breadth of any specific dye. Dyes with narrow E_{gap}^{opt} can capture photons from the longer-wavelength regions of the solar spectrum and facilitate ICT events. The orbital energies and E_{gap}^{opt} of all theoretically proposed molecules (and the reference molecule) are tabulated in Table S3 and plotted in Figure 3. The HOMO energies of
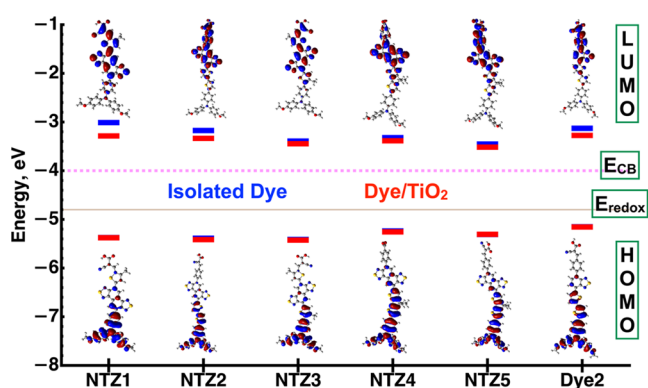

Figure 3. Schematic energy levels and frontier molecular orbitals of designed NTZ dyes (dyes/TiO$_2$ cluster), reference dye (**DYE2**) along with the conduction band energy of TiO$_2$ (E_{CB}) and the redox potential of the iodine electrolyte (E_{redox}). All of the results were obtained at the DFT/PBE0/6-311G(d,p) level of theory in dichloromethane solvent. The TiO$_2$ conduction band energy is taken at −0.5 V versus the normal hydrogen electrode and converted to a vacuum scale by the equation $E_{CB} = -|-0.5 + 4.5|$. E_{redox} is found via the equation $E_{redox} = -|0.35 + 4.5|$ with the redox potential of iodine being taken as 0.35 V versus NHE. Both conversions from NHE to vacuum used a constant of 4.5 V, and it should be noted that the values of TiO$_2$[3,14,67,68] and the iodine electrolyte[3,67,69] are only gross approximations that are widely accepted values in the literature.

the designed molecules lie between −5.07 eV (**NTZ4**) and −5.34 eV (**NTZ1**), whereas the LUMO energies spread between −3.05 eV (**NTZ4**) and −3.38 eV (**NTZ3**). The computed E_{gap}^{opt} is 2.09 eV for **DYE2**, 2.03 eV for **NTZ1**, 1.91 eV for **NTZ2**, 1.85 eV for **NTZ3**, 2.02 eV for **NTZ4**, and 1.87 eV for **NTZ5**. The obtained results indicate that the NTz-based molecules have a lower E_{gap}^{opt} than the reference BTD-based molecule (**DYE2**). The trend of the gap value is as follows: **NTZ3** < **NTZ5** < **NTZ2** < **NTZ4** < **NTZ1** < **DYE2**. Likewise, **NTZ5** shows a low-optical-energy gap due to the fused π-conjugated cyclopentadithiophene (CPDT) bridge. The use of CPDT increases the coplanarity between the dye building blocks, which facilitates lower-energy charge transfer. The direct comparison of BTD to NTz is possible by comparing **DYE2** and **NTZ2**, which shows a 0.18 eV more narrow E_{gap}^{opt} when NTz is used. Additionally, even when the dithiophene π-linker of **DYE2** is removed and BTD is substituted for **NTZ1**, a smaller E_{gap}^{opt} value is observed with the NTZ dye despite a shorter π-conjugated system. Thus, the designed dye molecules are good potential candidates for

DSSCs compared to the reference dye. We also have computed the singly occupied molecular orbital (SOMO) energies of the cationic state of the designed dyes (Table S3) and found that most of the designed molecules have lower SOMO values (−6.31 to −5.86 eV) relative to **DYE2** (−5.89 eV) except **NTZ4** and **NTZ5**. The obtained results revealed that the cationic state of most NTz-based dyes is more stable than that of the reference molecule. The NTz unit acts as an auxiliary acceptor to reduce the E_{gap}^{opt} up to 0.24 eV. The narrowest optical energy gap was obtained using an auxiliary acceptor and a five-membered ring (like thiophene) as a π-bridge between A′ and the anchoring group.

Charge transfer will be more efficient if there is a relatively strong electronic coupling between the adsorbed dye and the TiO$_2$ film due to interactions of the dye acceptor group and TiO$_2$ substrate shown via the LUMO orbital position. Qualitative coupling could be estimated by reducing the LUMO energy level of the adsorbed dye.[65,66] In this study, all bounded dyes show decreased LUMO energy levels indicating the possibility of efficient charge transfer from the dye to TiO$_2$.

The electron density distribution maps of the HOMOs and LUMOs of the studied dyes are depicted in Figure 3. In all of the cases, the HOMO is mainly delocalized on the donor TAA unit, spreads over the π-linker, and extends to the auxiliary acceptor (NTz or BTD) in some cases. The LUMO orbitals are located on the A′−π−A structure with some distribution over the π-linker near the TAA. Thus, the distribution of both orbitals confirms that sufficient overlap between the donor and acceptor motifs is present as is needed to facilitate efficient ICT upon excitation. As a result, the excitation of an electron from the HOMO to the LUMO will allow for maximum photoinduced ICT.[23,70] However, in **NTZ4**, the LUMO is localized primarily over the NTz fragments, which might hinder the flow of electrons to the BA group and then to the CB of TiO$_2$.

Electronic Absorption Spectra. The light absorption properties can be characterized by the absorption maximum (λ_{max}), oscillator strength (f), and orbital contributions in the respective excitation. An insight into those parameters of the sensitizer represents a crucial factor in understanding and evaluating its photophysical properties. DSSCs with the highest practical PCE value require that the sensitizer absorption spectra absorb up to ∼950 nm of the solar spectrum.[71] The simulated UV−vis absorption spectra of the isolated dyes and the dye−TiO$_2$ complexes (see the supporting information, Figure S2) in DCM solvent are presented in Figure 4. Maximum absorption wavelengths (λ_{max}), oscillator strengths (f), and transition characters with major transitions for the dyes are collected in Table 2.

The experimental λ_{max} of **DYE2** in the DCM solvent is 515 nm, and the computed vertical excitation value with OT-ωB97XD/6-311G(d,p)//B3LYP is ca. 517 nm. The λ_{max} values for all other designed dyes are greater than the **DYE2** value, and the numbers are ca. 542, 537, 575, 561, and 578 nm for **NTZ1**−**NTZ5**. All of the designed NTZ dyes exhibit a red shift compared to **DYE2**, suggesting that these dyes can be used in DSSCs for the efficient harvesting of more photons from the solar spectrum than **DYE2**. The trend of the computed values is as follows: **NTZ5** > **NTZ3** > **NTZ4** > **NTZ1** > **NTZ2** > **DYE2**. In all of the designed dyes, the BTD unit of **DYE2** was replaced by the NTz unit, resulting in a large red shift (>50 nm). A larger shifting of the ICT band in **NTZ5** and **NTZ3** is observed due to the synergistic effect from the
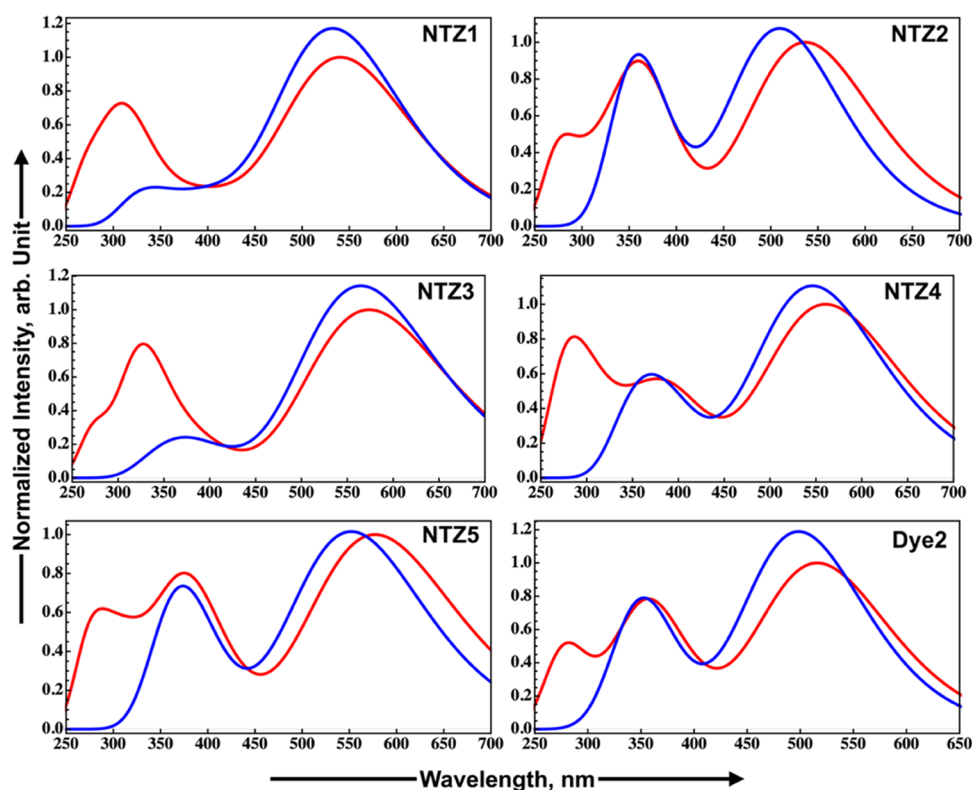
Figure 4. UV−vis absorption spectra of the proposed dyes. Red and blue lines indicate the UV−vis spectrum of the isolated dyes and dyes on TiO$_2$, respectively, with the curves generated by setting the half-width at half-height to 0.11 eV.

Table 2. Electronic Absorption Spectra Result in Dichloromethane Solvent at the TD-DFT OT-ωB97XD/6-311G(d,p)// PBE0/6-311G(d,p) Level of Theory with ω = 0.14 Bohr[a,b]

dyes	excitation	λ_{max} (nm)	λ_{max} (eV)	f	major contribution
NTZ1	S$_0$ → S$_1$	541.87	2.29	1.45	H → L (61.1%), H^{-1} → L (29.0%)
	S$_0$ → S$_2$	418.50	2.96	0.22	H^{-1} → L (49.0%), H → L (13.6%)
	S$_0$ → S$_3$	369.47	3.36	0.14	H^{-1} → L^{+1} (46.8%), H → L^{+1} (19.0%)
NTZ2	S$_0$ → S$_1$	536.98	2.31	1.80	H^{-1} → L (40.4%), H → L (38.3%)
	S$_0$ → S$_2$	397.04	3.12	0.16	H^{-2} → L(23.1%), H → L^{+3}(21.8%), H → L (8.2%)
	S$_0$ → S$_3$	364.34	3.40	1.30	H → L^{+3} (22.1%), H^{-1} → L^{+1} (14.6%)
NTZ3	S$_0$ → S$_1$	574.11	2.16	1.74	H → L (45.5%), H^{-1} → L (44.5%)
	S$_0$ → S$_3$	383.00	3.24	0.27	H^{-1} → L^{+1} (42.4%), H → L (16.5%)
	S$_0$ → S$_4$	355.21	3.49	0.14	H^{-1} → L^{+2} (43.4%), H → L^{+2} (34.4%)
NTZ4	S$_0$ → S$_1$	561.22	2.21	1.50	H → L (57.5%), H^{-1} → L (29.1%)
	S$_0$ → S$_2$	401.97	3.08	0.56	H → L^{+2} (27.5%), H → L^{+1} (18.3%)
	S$_0$ → S$_3$	359.93	3.44	0.40	H → L^{+2} (21.9%), H^{-2} → L (13.8%)
NTZ5	S$_0$ → S$_1$	577.48	2.15	1.77	H → L (52.1%), H^{-1} → L (26.3%)
	S$_0$ → S$_2$	405.52	3.06	0.31	H → L^{+3} (26.4%), H → L^{+2} (21.9%)
	S$_0$ → S$_3$	376.58	3.30	1.00	H → L^{+1}(21.8%), H → L^{+3} (19.7%)
	S$_0$ → S$_4$	363.40	3.41	0.11	H → L (31.6%), H → L^{+2} (18.1%)
DYE2	S$_0$ → S$_1$	516.56	2.40	1.55	H → L(46.1%), H^{-1} → L(35.2%), H → L^{+1} (5.4%)
	S$_0$ → S$_2$	376.52	3.29	0.29	H → L^{+2} (44.3%), H^{-2} → L (15.7%)
	S$_0$ → S$_3$	354.76	3.49	1.03	H^{-1} → L^{+1} (24.7%), H → L^{+1} (92.1%)

[a]Absorption bands with f > 0.1 and λ > 350 nm in the visible and near-UV regions for all dyes in CH$_2$Cl$_2$. [b]"S" indicates a state, "H" indicates HOMO, and "L" indicates LUMO.

CPDT π-linker and thiophene π-linker/π-bridge units, respectively.

The spectra of all of these dyes have two distinct absorption bands in the UV and visible regions. The absorption at shorter wavelengths ranging from 200 to 400 nm can be described by π−π* electronic transitions along with shorter range ICT events, and the longer wavelengths ranging between 400 and 1000 nm can be categorized by an ICT event from the donor unit to the acceptor unit. The absorption peaks at 400−1000 nm can be assigned to the S$_0$ → S$_1$ transition. Interestingly, similar absorption behavior was observed by the dye−TiO$_2$ complex and the isolated dyes. It is noted that the CT band of the DYE2−TiO$_2$ complex is blue-shifted in our calculations, which is parallel to the experimental observation. The values of
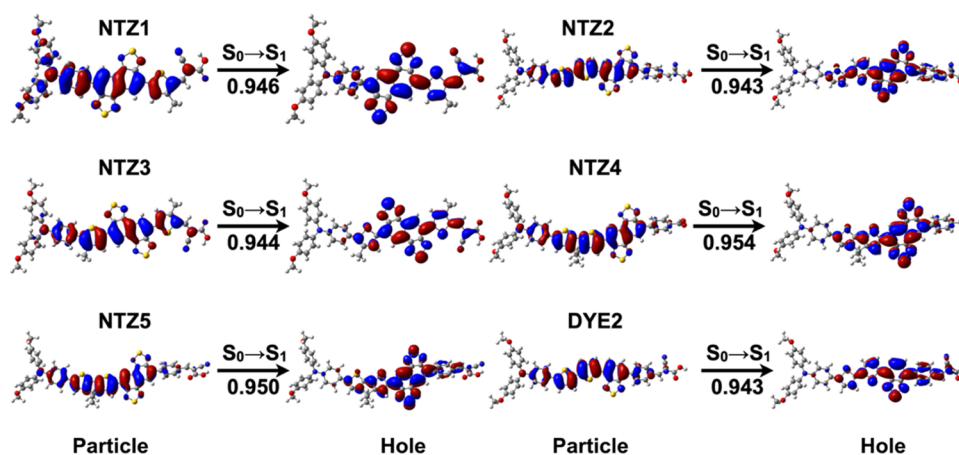
Figure 5. Visual mapping of the NTOs for $S_0 \rightarrow S_1$ of the designed dyes, including the occupation number for the transition from the particle to hole in dichloromethane as determined at the OT-ωB97XD/6-311G(d,p) level of theory. The isovalue is 0.02 au.

the CT bands of all of the designed NTZ dyes on TiO$_2$ are also blue-shifted.

After analyzing the data in Table 2, it is evident that most of the transitions are not solely contributions of the HOMO to LUMO transfers. We employed natural transition orbital (NTO) analysis[72] for a qualitative description of electronic excitation. In Figure 5, we plotted NTOs for $S_0 \rightarrow S_1$ transitions with their occupation number.

Intramolecular Charge Transfer. Charge-transfer distances (D_{CT}), t-index (t), overlap integral (S), Δr index (the measure of CT length), hole−electron Coulomb attractive energy (E_C), and dipole moment variation (μ_{norm}) were computed to characterize the charge-transfer properties of the isolated dyes (Tables 3 and S2).[73] A more positive value of t

Table 3. Computed Different ICT Parameters Such as Δr Index, t-Index, Overlapping Integral (S), the Distance between the Center of C^+ and C^- (D_{CT}), and the Change in the Dipole Moment Compared to the Ground State (μ_{norm})[a]

dyes	Δr (Å)	D_{CT} (Å)	μ_{norm} (Debye)	t (Å)	S (au)
NTZ1	6.79	3.364	12.911	−2.557	0.95
NTZ2	11.17	3.444	14.501	−4.423	0.97
NTZ3	8.04	2.969	11.662	−3.995	0.96
NTZ4	9.55	3.378	14.950	−3.640	0.96
NTZ5	11.53	3.510	15.826	−3.984	0.97
DYE2	10.95	2.732	12.505	−5.365	0.98

[a]All of the values are for $S_0 \rightarrow S_1$ excitation in the solvent dichloromethane.

represents a significant separation of the positive and negative electron density variations due to strong CT behavior. A larger D_{CT} value indicates that the CT distance is longer. D_{CT} (2.732 Å) and t-index (−5.365 Å) values of the reference molecule (**DYE2**) are lower than for the designed NTZ dyes. The trend of the t-index values of the isolated dyes is as follows: **NTZ1 > NTZ4 > NTZ3 > NTZ5 > NTZ2 > DYE2**. The excitations caused a significant variation in dipole moment values (μ_{norm}). The values of D_{CT} and the stronger Coulomb attractive energies of the NTz dyes are inversely correlated. Larger Δr and D_{CT} imply better ICT behavior, which could increase the probability of electron transfer to TiO$_2$. Small S values, overlapping between hole and electron centroids (C^+ and C^-), also imply better efficiency of charge transfer spatially.[62] The

qualitative description of the ICT phenomenon via different indices shows excellent consistency. Hence, using the NTz unit to replace the BTD unit in **DYE2** is an effective way to enhance the ICT character by increasing the CT state separation. One can conclude that the designed NTz dyes have better charge-transfer characteristics than **DYE2**, which encourages the evaluation of these sensitizers in DSSCs.

Excited-State Lifetime and the Radiative Lifetime. The dye excited-state lifetime is a critical parameter that affects the electron injection efficiency into TiO$_2$ with longer excited-state lifetimes leading to higher injection quantum yields. We applied a fast and efficient screening approach[74] to identify the nature of the NTz-based dyes' first excited-state lifetime (τ_e) using the relationship $\tau_e = 1.499/(fE^2)$), where E (cm^{-1}) is the excitation energy for S_1 and f represents the oscillator strength for the respective state. The τ_e values are tabulated in Table 4 and **DYE2** (2.56 ns) has the lowest value among the NTz-based dyes.

Table 4. Computed Excited-State Lifetime (τ_e), Radiative Lifetime (τ_{em}), Excited-State Oxidation Potential (E_{dye*}), Free Energy of Electron Injection (ΔG_{inject}), Light-Harvesting Efficiency (LHE), Dye Adsorption Energy (E_{ads}), and the Change in the Conduction Band of TiO$_2$ after the Dye Adsorption (ΔE_{CB} in meV) of the NTZ-Based Dyes and DYE2[a]

dyes	τ_e	τ_{em}	E_{dye*}	ΔG_{inject}	E_{ads}	LHE	ΔE_{CB}
NTZ1	3.75	4.32	−3.05	−0.95	−2.21	0.96	272
NTZ2	2.89	3.55	−2.85	−1.15	−2.23	0.98	285
NTZ3	3.23	4.06	−3.07	−0.93	−2.25	0.98	271
NTZ4	3.59	4.37	−2.86	−1.14	−2.30	0.97	252
NTZ5	3.13	3.73	−2.93	−1.07	−2.23	0.98	285
DYE2	2.56	3.65	−2.75	−1.25	−2.17	0.97	160

[a]All energies are in eV except ΔE_{CB} and lifetime is in ns.

On the other hand, the τ_e values of the designed NTZ dyes lie between 2.89 and 3.75 ns, and the trend is **NTZ1 > NTZ4 > NTZ3 > NTZ5 > NTZ2**. This outcome indicates that substituting the BTD unit with the NTz unit is a fruitful method to enhance the excited-state lifetime of the dyes.

We also have computed the radiative lifetime (τ_{em}) of all of the designed NTz dyes and **DYE2** using the Einstein transition model[75]

$$\tau_{em} = \frac{c^3}{2(E_{flu})^2 f} \tag{1}$$

where c represents the speed of light, E_{flu} indicates the fluorescence transition energy based on the optimized first excited-state (S_1^{ex}) structure, and f stands for the oscillator strength corresponding to S_1^{ex}. All of the computed data related to lifetime are tabulated in Table 4. The values of τ_{em} of NTz-based dyes are much longer compared to DYE2, except NTZ2. The results indicate that using a benzene ring after the NTz or BTD unit in conjunction with CA as an anchoring group decreases the radiative lifetime. In contrast, either using BA as an anchoring group or thiophene with CA provides an extended emission lifetime.

As photostability is one of the critical parameters for the longevity of solar cell devices,[76] we evaluated the stability of the photoexcited dyes. In principle, a photoexcited dye with a lower-energy excited state is desired to be less active in undergoing photochemical reactions and vice versa.[77] To assess this energy qualitatively, we implemented an efficient approach based on the excited-state oxidation potential (ESOP; aligned S_1) and the ground-state oxidation potential (GSOP). Figure 6 outlines the ESOP, GSOP, and FMOs of
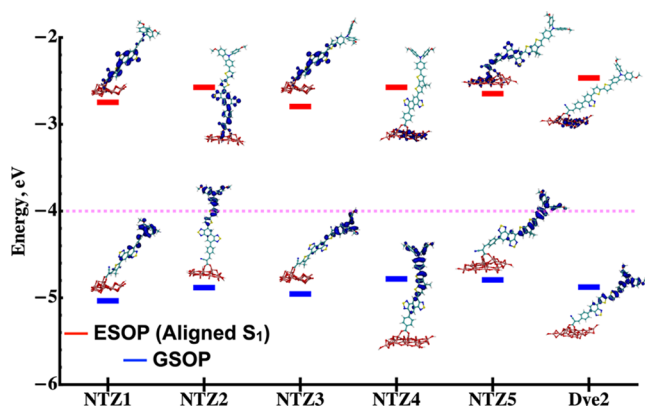

Figure 6. Excited-state oxidation potential (ESOP) and ground-state oxidation potential (GSOP) along with the HOMO (bottom panel) and LUMO (top panel) of dye−TiO$_2$ cluster complexes. ESOP aligned with first excitation energy, $S_0 \rightarrow S_1$. The dotted magenta line indicates the CB edge of TiO$_2$, and the isovalue is 0.02 au.

dye−TiO$_2$ cluster complexes. Since ESOP computations are expensive, we estimated the values using the GSOP and the vertical excitation energy via the equation

$$ESOP \cong GSOP - E_{S_1}$$

where E_{S_1} is the first excitation energy of the dye molecule.[56,78] Figure 6 outlines the difference between GSOP and ESOP, a gradient in charge transfer, which is highest for the DYE2 and lowest for the NTZ5. Although almost all of the dyes show similar ESOP, NTZ3 is relatively closer to the CB of TiO$_2$, which ensures less thermal energy waste upon charge transfer.

The display of the HOMO and LUMO of the dye−TiO$_2$ cluster complexes is presented in Figure 6 along with the ground- and excited-state oxidation potentials. The HOMO is mainly delocalized on the TAA and π-linker, similar to the isolated dyes, whereas the LUMO is distributed either on the NTz unit through the TiO$_2$ cluster (NTZ1, NTZ2, NTZ3, and NTZ5) or only in the TiO$_2$ cluster region (NTZ4 and DYE2). It is notable to mention that the dyes with a BA anchoring

group show only the later pattern of the LUMO distribution. However, it is generally accepted that strong coupling of the LUMO of the isolated dye and CB of TiO$_2$ is more favorable, ensuring the fastest charge transfer of an electron from the dye to the semiconductor.[75,79] Therefore, the designed dyes with CA groups could be efficient potential candidates to use in DSSCs to enhance the electron injection from the sensitizer to the CB of TiO$_2$.

Photophysical Properties. *Prediction of Short-Circuit Current Density (J_{SC}).* The equation $J_{SC} = \int LHE(\lambda)\cdot\Phi_{inject}\eta_{collect}\,d\lambda$ is used to estimate short-circuit current density. In DSSCs, electron injection events can be elucidated by the charge-transfer (CT) process. CT has been associated with the electron injection rate (Φ_{inject}) or efficiency, which may be quantified by the free-energy change for electron injection (ΔG_{inject}) in DSSCs. The injection energy can be calculated as[13] $\Delta G_{inject} = E_{dye*} - E_{CB}$, where $E_{CB} = -4.0$ eV. The oxidation potential of the excitation of the dye (E_{dye*}) can be computed from the relation, $E_{dye*} = E_{dye} - \lambda_{max}$, assuming that the electron injection occurs from the unrelaxed excited state[13,80] where E_{dye} and λ_{max} are the redox potential of the ground state and first vertical energy, respectively. Notably, the E_{dye*} value will be larger in energy than experimentally measured (i.e., the absolute ΔG_{inject} values will be overestimated) since the lower-energy absorption curve onset is the commonly used parameter for calculating E_{dye*} values; however, absorption curve onset values are not easily obtained computationally and λ_{max} values are used in this instance for a relative comparison between the dyes. All of the computed photophysical properties are tabulated in Table 4, and according to Koopmans' theorem, $E_{dye} = -E_{HOMO}$. All of the designed dyes show negative values of ΔG_{inject}, which implies that the excited states of the dyes lie above the CB edge of TiO$_2$ with an effective charge-transfer excitation character.[81] The ΔG_{inject} values of the designed dyes have lower values compared to DYE2. Light-harvesting efficiency (LHE) can be estimated using the oscillator strength (f) of the first excited state as LHE = $1 - 10^{-f}$. The table depicts all of the computed values used to estimate J_{SC}. The LHE values are closely grouped with DYE2.

Dye regeneration efficiency (η_{reg}) is also critical to DSSC device performances and can be related to the driving force of regeneration (ΔG_{reg}) between the oxidized dyes and the iodine electrolyte. ΔG_{reg} can be computed using the relationship: $\Delta G_{reg} = |E_{redox}| - |E_{dye}|$ where E_{redox} is the redox potential of iodine electrolytes. In this work, we assumed its value to be -4.85 eV (see Figure 3 caption). Computed values of ΔG_{reg} of all of the dyes are negative, which suggests spontaneity of the process. NTZ1 (-0.49) and NTZ3 (-0.38) possess higher regenerative driving forces than DYE2, whereas NTZ2, NTZ4, and NTZ5 have competitive ΔG_{reg} values.

Prediction of Open-Circuit Voltage (V_{OC}). The open-circuit voltage (V_{OC}) is one of the salient features of DSSCs and is estimated by eq 2. The equation shows that dyes with larger ΔE_{CB} values can cause a significant variation in V_{OC}.

$$V_{OC} = \frac{E_{CB}}{q} + \frac{kT}{q}\ln\left(\frac{n_c}{N_{CB}}\right) - \frac{E_{redox}}{q} \tag{2}$$

The shift of the CB edge of TiO$_2$ after dye adsorption can be computed qualitatively using the method reported by Ronca et al.[82] and can be expressed as $\Delta E_{CB} = \Delta E_{CB-solv} + \Delta E_{CB-ions} + \Delta E_{CB-dye}$, where $\Delta E_{CB-solv}$, $\Delta E_{CB-ions}$, and ΔE_{CB-dye} represent the
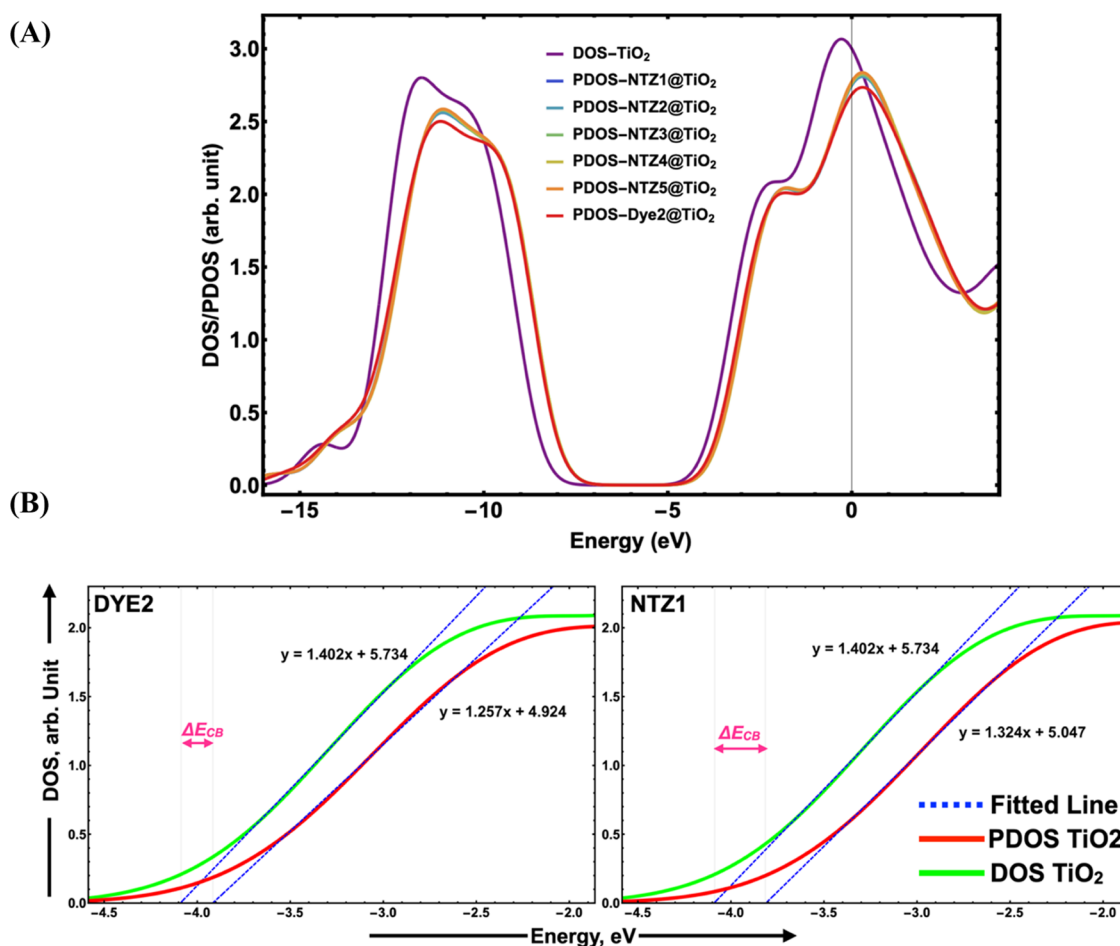
Figure 7. Shift in the edge of the conduction band of TiO_2 after dye adsorption on a TiO_2 cluster. (A) PDOS of all of the dyes compared to TDOS of bare TiO_2 at FWHM = 1.36 eV. (B) TDOS plot of the bare $(TiO_2)_{16}$ cluster, and the PDOS of the $(TiO_2)_{16}$ cluster after dye adsorption with fitted lines on the sigmoidal portion of the curves.

shift that stems from solvent, ions, and adsorbed dyes, respectively. Under the same experimental condition, the effects of solvents and ions on dye properties are assumed to be constant. Hence, ΔE_{CB} can be estimated based on the shift of the TiO_2 CB from its pristine band to a new energy after the adsorption of the dye. The total density of states (TDOS) of TiO_2 and partial density of states (PDOS) of the dye–TiO_2 complex were analyzed to evaluate ΔE_{CB}. The energy difference between the linear fit of the straight portion of sigmoid curves of TDOS and PDOS of TiO_2 is the ΔE_{CB}. The TDOS and PDOS of the $(TiO_2)_{16}$ cluster of all of the dyes are depicted in Figure 7A, and it is evident that the CB edge (CBE) of the TiO_2 cluster is shifted upward with respect to the bare surface in all cases. This shift indicates an increase in electron density from the dye to the CB of TiO_2. The shift of the CBE in **NTZ1** and **DYE2** is described in Figure 7B and all other dyes are included in Figure S3 (Supporting Information). We have found that the ΔE_{CB} value of **DYE2** is 160 meV, whereas the designed NTz dyes lie between 252 and 286 meV, which is at least 92 meV higher than **DYE2**. The results suggest that the NTz dyes will enhance the V_{OC} value in comparison to **DYE2**. Also, we performed NPA calculation based on the PBE0 density matrix for the dye, TiO_2, and dye@ TiO_2 cluster models with dichloromethane as the solvent. The obtained values indicate that approximately 0.539–0.572 electrons are transferred from mainly the carboxylate group

of the dyes to the two nearest Ti atoms when the dye is bound to the TiO_2 cluster (see the Supporting Information, Table S5). The NPA results indicate that the NTz dyes have a higher preference for interacting with the TiO_2 cluster than **DYE2**, which contains BTD. Having found intriguing computed properties for NTz-based dyes relative to BTD-based dyes, we sought to synthesize comparable analogues using these building blocks.

■ EXPERIMENTAL METHODS

General Synthesis Information. All of the reagents and solvents used in this study were purchased from Sigma-Aldrich, Acros Organics, or Thermo-Fischer Scientific. Heated reactions were immersed in an oil bath. ^1H NMR spectra were recorded on a Bruker 400 MHz spectrometer using deuterated solvents. J values are in Hz and chemical shifts were in ppm using the residual solvent as a reference (CHCl$_3$ = 7.26 ppm). Singlet (s), doublet (d), quartet (q), apparent (ap), and multiplet (m) were designated as ^1H NMR signal splitting patterns. The absorption spectrum was recorded on a Cary 5000 UV–Vis–NIR spectrophotometer. Silica gel (230–400 mesh) was used for column chromatography separations. Electrospray ionization (ESI) high-resolution mass spectrometry (HRMS), quadruple-TOF was used to obtain the data both in positive mode with a Waters Synapts XS. The mass analyzer was set to the 200–3000 Da range. Infrared spectra

were recorded with an Agilent Cary 660 attenuated total reflection-Fourier transform infrared (ATR-FTIR) spectrometer.

1,5-Bis(p-toluenesulfonamido)naphthalene (2). The compound was synthesized on a 10-g scale from naphthalenediamine (**1**) by following a reported procedure.[83] Pure compound **2** was obtained with a 77% yield as a solid as previously reported. This compound was carried forward as done previously in the literature.

2,6-Dinitro-1,5-bis(p-tolylsulfonylamino)naphthalene (3). The compound was synthesized via a modification to the previously reported procedure.[83] Compound **2** (9.0 g, 19.3 mmol) and sodium nitrite (0.44 g, 6.4 mmol) in acetic acid (91 mL) were cooled to 0 °C in an ice bath. Then, a solution of 70% HNO_3 (13.5 mL) in acetic acid (9 mL) was added dropwise, causing a temperature increase from 0 °C to 25 °C. The mixture was stirred at room temperature for 24 h. Then, excess K_2CO_3 (aq.) was added to neutralize the reaction mixture, and then, the brownish product was filtered, washed with cold acetic acid and ethanol, dried under vacuum overnight, and then recrystallized from pyridine and water (1:2) to give compound **3** as a yellow solid with a 63% yield (6.7 g, 12.0 mmol). Spectroscopic data agrees with the literature report.

1,5-Diamino-4,8-dinitronapthalene (4). The compound was synthesized following the reported procedure.[83] The product was obtained in quantitative yield as a dark purple solid. Spectroscopic data agrees with the literature report.

1,2,5,6-Napthalenetetraamine Tetrahydrochloride salt (5). The compound was synthesized by following the reported procedure.[84] Gray-colored, shiny crystals of 1,2,5,6-naphthalenetetramine tetrahydrochloride (Yield: 80%) were immediately used in the next reaction. Spectroscopic data agrees with the literature report.

Naphtho[1,2-c:5,6-c']bis[1,2,5]thiadiazole (NTz). **NTz** was synthesized as described in the literature for an analogous compound.[85] To a solution of compound **5** (0.09 g, 0.26 mmol) in dry pyridine (2.6 mL), N-thionylaniline (0.06 mL, 0.52 mmol) and trimethylsilyl chloride (0.06 mL, 0.47 mmol) were added under nitrogen. Then, the solution was stirred at 80 °C for 16 h before being poured into ice water. The resulting solid was filtered and washed with ethanol to give 45 mg (0.18 mmol) of the rust-colored solid product (yield: 68%).[86] Spectroscopic data agrees with the literature report.[86]

5,10-Bis(4,4,5,5-tetramethyl-1,3,2-dioxaborolan-2-yl)-naphtho[1,2-c:5,6c']bis([1,2,5] thiadaz-ole) ((Bpin)₂NTz). (**Bpin**)₂**NTz** was synthesized according to the reported procedure.[87] Spectroscopic data agrees with the literature report.

Methyl-4-(10-(4-((4-(hexyloxy)phenyl) (4-(pentyloxy)-phenyl)amino)phenyl)naphtho [1,2-c:5,6-c'] bis ([1,2,5]-thiadiazole)-5-yl)benzoate (7). Compound (**Bpin**)₂**NTz** (0.015 g, 0.03 mmol), methyl-4-bromobenzoate (0.03 mmol), TAA–Br (**6**) (0.3 mmol), $Pd[(tBu)_3P]_2$ (0.003 g, 6 μmol), and K_2HPO_4 (0.049 g, 9.45 mmol) were dissolved in THF (1.2 mL) and H_2O (0.06 mL). The mixture was stirred 12 h at 90 °C under nitrogen and then cooled to room temperature. The mixture was extracted with ethyl acetate and water. The organic layer was separated and concentrated under reduced pressure. The crude product was purified by a silica column with the 25−50% DCM gradient with the remainder as hexanes (Yield: 35%, 8 mg, 0.0097 mmol). λ_{max} (abs) = 506 nm (Figure 8), ¹H NMR (400 MHz, CDCl₃) δ 9.08 (s, 1H),
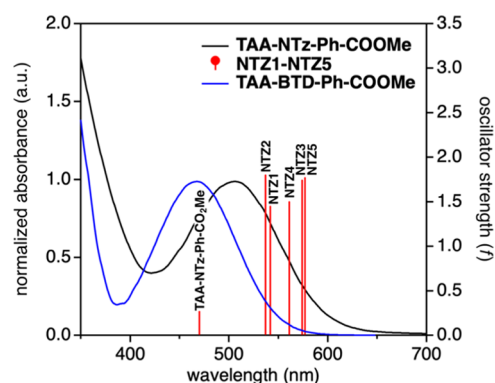

Figure 8. Absorption curve of **TAA-NTz-Ph-COOMe** (**7**) (black line), **TAA-BTD-Ph-COOMe** (blue line), and the lowest-energy vertical transitions for dyes NTZ1−NTZ5 (red lines) in dichloromethane.

8.99 (s, 1H), 8.25−8.21 (ap q, 4H), 7.99 (d, J = 8.8 Hz, 2H), 7.15 (d, J = 9.0 Hz, 2H), 7.09 (d, J = 8.8 Hz, 2H), 6.86 (d, J = 9.0 Hz, 2H), 3.99−3.96 (m, 7H), 1.59−0.82 (m, 22H) (Figure S4). IR (cm⁻¹): 3040, 3002, 2950, 2920, 2852, 1720, 1627, 1598, 1500, 1455, 1276, 1237, 1196 and 826. MS (ESI) m/z: $[M]^+$ calculated for $C_{48}H_{47}N_5O_4S_2$ (821.3069); found 821.3013.

Synthesis. Interestingly, only one **NTz**-based dye with a carboxylic acid anchoring group is reported to have been synthesized in the literature based on a SciFinder search.[42] Synthesis of the target dyes was undertaken having found interesting computational properties of the dyes. Initially, a simplified target dye (a triarylamine donor, NTz auxiliary acceptor, phenyl π-spacer, and carboxylic acid acceptor) is targeted owing to the phenyl groups often imparting maximal stability on π-bridges during synthesis in our experience. This model system allows for the probing of synthetic accessibility of the dyes. Initially, the known literature route to the model dye was followed with the tosylation of **1**,[83] nitration of **2**,[83] deprotection of **3**,[83] nitro reduction of **4**,[84] **NTz** formation from **5**,[85,86] and double borylation of **NTz** through an Ir-catalyzed C−H activation[87] to give the key coupling partner (**Bpin**)₂**NTz** (Scheme 1). After the significant screening of routes and conditions (Schemes S2 and S3; Table S6), a one-pot three-component Suzuki coupling of (**Bpin**)₂**NTz**, **6**, and methyl-4-bromobenzoate awarded compound **7** (**TAA-NTz-Ph-COOMe**) in a 35% yield with a slight inseparable impurity in the ¹H NMR spectrum. All other routes led to decomposition of the **NTz** building block or a large number of challenging to separate products forming in the reaction. Compound **7** is found to have instability on SiO_2 and Al_2O_3 chromatography media and had to be rapidly purified with SiO_2 to avoid substantial decomposition. Attempts to hydrolyze the ester to give the carboxylic acid, which is needed for functional DSSC devices, were unsuccessful and resulted in decomposition of **7** before the hydrolysis reaction could take place (Scheme S4 and Table S4). However, **7** could be studied by absorption spectroscopy and compared to computational results (Figure 8). Compound **7** has a broad absorption feature from 400 to 650 nm that is indicative of an ICT dye. This is in good agreement with the predicted orbital distributions of **NTZ1−NTZ5**, which show the HOMO on the TAA region with some incorporation on the NTz building block and the LUMO on the NTz-acceptor portions. This regional separation of the orbitals on the dye is typical of ICT dyes.

Scheme 1. Synthetic Scheme to Synthesize TAA-NTz-Ph-COOMe (7)
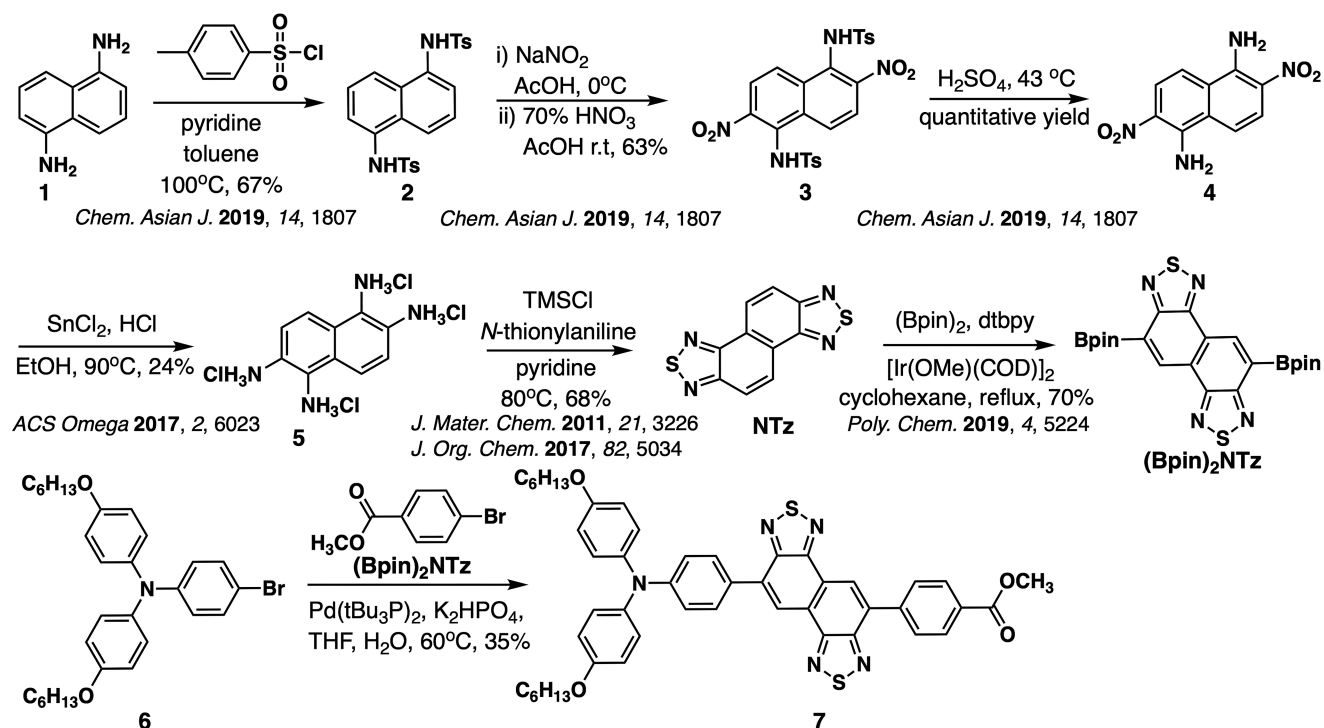
The computed orbital positioning, energetics, and spectroscopic properties of synthesized dye 7 were analyzed. We found that the energetics of the FMOs have a similar HOMO energy to **NTZ1** and the most positive LUMO energy of all of the dyes studied, including the benchmark dye (Figure S5). The HOMO is mainly delocalized on the TAA with some contribution on the NTz group, whereas LUMO is distributed onto the NTz unit with some contribution on the benzoic acid acceptor (Figure S5). The low-energy absorption maximum (λ_{max}) of 7 is at 506 nm. The computed λ_{max} is also in good agreement with the experimental value (within 36 nm, Figure S6), which further validates the computational approach used in this study. Notably, the computed NTz-based dyes have vertical transition energies more red-shifted than 7, which would be expected based on the use of thiophene building blocks with lower resonance stabilization energies than benzene groups allowing for lower-energy ICT events. Additionally, the computed dyes use cyanoacrylic acid groups that are most strongly electron withdrawing than the carboxylic ester of 7. Thus, the **NTZ1** dyes should be more red-shifted than 7 as predicted. Overall, the model compound synthesized (7) indicates that the computational data is reasonable given the ICT nature predicted and observed and the relative predicted vertical transitions to the observed λ_{max}. A BTD-based analogue to **TAA-NTz-Ph-COOMe** was synthesized in a similar manner to known **C264**[88] (the carboxylic acid derivative). This allows for a direct comparison of the optical properties of the BTD and NTz building blocks, which reveals a ~60 nm red shift of the dye absorption curve onset when the NTz building block is used relative to the BTD building block. If the synthetic challenges present could be overcome, then the **NTZ1−NTZ2** target dyes would be interesting to employ in DSSC devices. Notably, compound 7 is stable for more than a year under ambient conditions with no indication of decomposition as a solid. This suggests that the synthetic

challenges encountered are likely due to conditions of the reaction and purification protocols. If a suitable methodology could be found to directly arrive at the desired dyes from **NTz**, **NTzBr$_2$**, or (**Bpin**)$_2$**NTz** cleanly, then this class of sensitizers could be of significant interest to the DSSC community.

■ CONCLUSIONS

We computationally designed five triphenylamine derivative dyes using the NTz unit as an auxiliary acceptor between a donor-π-linker and π-spacer-terminal acceptor (cyanoacrylic acid or benzoic acid) for their potential application in DSSCs. Systematic DFT and TD-DFT level studies were carried out to compute various structure−property relationships and photophysical properties of isolated dyes, along with the dye−TiO$_2$ interface. The use of NTz as an auxiliary acceptor provides an efficient way to broaden the optical response. Compared to the reference dye, all of the designed dyes possess a narrow optical energy gap (1.85−2.03 eV). The critical parameters related to J_{SC} and V_{OC} such as the driving force of electron injection (ΔG_{Inject}), the spontaneity of dye regeneration (ΔG_{Reg}), CT length (d_{CT}), and the shift of CB of TiO$_2$ (ΔE_{CB}) were computed. The obtained results implied that the use of the NTz unit improves the absorption spectrum and charge separation, d_{CT}, due to its high planarity. The ΔE_{CB} value is higher for NTz dyes, which suggests that the V_{OC} of DSSC devices should be higher than the value for the benchmark **DYE2**. The results obtained from the study suggested that the designed dyes are interesting candidates for efficient DSSCs. A model compound (7) was synthesized, which confirms many of the predicted characteristics, including an ICT nature and reasonably well-correlated vertical transition energies. The synthetic challenges in accessing the computed dyes are an excellent opportunity for method developments aimed at mild, clean reactions and purifications that can overcome the issues

encountered herein when employing traditional cross-coupling chemistry, hydrolysis chemistry, and chromatography.

■ ASSOCIATED CONTENT

Ⓢ Supporting Information

The Supporting Information is available free of charge at https://pubs.acs.org/doi/10.1021/acs.jpcc.2c02117.

Method validation, tuning of the ω parameter, additional description of methods, absorption configuration of dyes@TiO$_2$, shift in conduction band energy of TiO$_2$ of all of the dyes, NPA results, optimized coordinates for all of the studied systems, attempted synthetic routes, and synthetic protocols (PDF)

■ AUTHOR INFORMATION

Corresponding Authors

Jared H. Delcamp − *Coulter Hall, Department of Chemistry, University of Mississippi, University, Mississippi 38677, United States;* ⓘ orcid.org/0000-0001-5313-4078; Phone: 662-915-5332; Email: delcamp@olemiss.edu

Jerzy Leszczynski − *Interdisciplinary Center for Nanotoxicity, Department of Chemistry, Physics and Atmospheric Sciences, Jackson State University, Jackson, Mississippi 39217, United States;* ⓘ orcid.org/0000-0001-5290-6136; Phone: +1 601 979 3723; Email: jerzy@icnanotox.org; Fax: +1 601 979 7823

Authors

Juganta K. Roy − *Interdisciplinary Center for Nanotoxicity, Department of Chemistry, Physics and Atmospheric Sciences, Jackson State University, Jackson, Mississippi 39217, United States;* ⓘ orcid.org/0000-0002-3646-5593

Ravinder Kaur − *Coulter Hall, Department of Chemistry, University of Mississippi, University, Mississippi 38677, United States;* ⓘ orcid.org/0000-0002-9394-4451

Andrew Daniel − *Coulter Hall, Department of Chemistry, University of Mississippi, University, Mississippi 38677, United States*

Alexandra Baumann − *Coulter Hall, Department of Chemistry, University of Mississippi, University, Mississippi 38677, United States;* ⓘ orcid.org/0000-0001-7435-5689

Qing Li − *Coulter Hall, Department of Chemistry, University of Mississippi, University, Mississippi 38677, United States;* ⓘ orcid.org/0000-0001-6723-5195

Complete contact information is available at:
https://pubs.acs.org/10.1021/acs.jpcc.2c02117

Notes

The authors declare no competing financial interest.

■ ACKNOWLEDGMENTS

■ REFERENCES

(1) Gong, J.; Li, C.; Wasielewski, M. R. Advances in Solar Energy Conversion. *Chem. Soc. Rev.* **2019**, *48*, 1862−1864.

(2) REN21. *Global Status Report, Renewable 2017*, 2017; Vol. 72.

(3) Hagfeldt, A.; Boschloo, G.; Sun, L.; Kloo, L.; Pettersson, H. Dye-Sensitized Solar Cells. *Chem. Rev.* **2010**, *110*, 6595−6663.

(4) Hagfeldt, A.; Grätzel, M. Molecular Photovoltaics. *Acc. Chem. Res.* **2000**, *33*, 269−277.

(5) Kar, S.; Roy, J. K.; Leszczynski, J. In Silico Designing of Power Conversion Efficient Organic Lead Dyes for Solar Cells Using Todays Innovative Approaches to Assure Renewable Energy for Future. *npj Comput. Mater.* **2017**, *3*, No. 22.

(6) O'Regan, B.; Grätzel, M. A Low-Cost, High-Efficiency Solar Cell Based on Dye-Sensitized Colloidal TiO2 Films. *Nature* **1991**, *353*, 737−740.

(7) Grätzel, M. Recent Advances in Sensitized Mesoscopic Solar Cells. *Acc. Chem. Res.* **2009**, *42*, 1788−1798.

(8) Raga, S. R.; Barea, E. M.; Fabregat-Santiago, F. Analysis of the Origin of Open Circuit Voltage in Dye Solar Cells. *J. Phys. Chem. Lett.* **2012**, *3*, 1629−1634.

(9) Liu, Y. F.; Guan, J.; Hu, D.; Du, L.; Sun, H.; Gao, J.; Zhao, J.; Lan, Z. Computational Investigation of Acene-Modified Zinc-Porphyrin Based Sensitizers for Dye-Sensitized Solar Cells. *J. Phys. Chem. C* **2015**, *119*, 8417−8430.

(10) Ding, I.-K.; Zhu, J.; Cai, W.; Moon, S.-J.; Cai, N.; Wang, P.; Zakeeruddin, S. M.; Grätzel, M.; Brongersma, M. L.; Cui, Y.; McGehee, M. D. Plasmonic Dye-Sensitized Solar Cells. *Adv. Energy Mater.* **2011**, *1*, 52−57.

(11) Roy, J. K.; Kar, S.; Leszczynski, J. Revealing the Photophysical Mechanism of N, N′-Diphenyl-Aniline Based Sensitizers with the D-D-π-A Framework: Theoretical Insights. *ACS Sustainable Chem. Eng.* **2020**, *8*, 13328−13341.

(12) Hardin, B. E.; Snaith, J.; Mcgehee, M. D. The Renaissance of Dye-Sensitized Solar Cells. *Nat. Photonics* **2012**, *6*, 162−169.

(13) Katoh, R.; Furube, A.; Yoshihara, T.; Hara, K.; Fujihashi, G.; Takano, S.; Murata, S.; Arakawa, H.; Tachiya, M. Efficiencies of Electron Injection from Excited N3 Dye into Nanocrystalline Semiconductor (ZrO 2, TiO 2, ZnO, Nb 2 O 5, SnO 2, In 2 O 3) Films. *J. Phys. Chem. B* **2004**, *108*, 4818−4822.

(14) Muñoz-García, A. B.; Benesperi, I.; Boschloo, G.; Concepcion, J. J.; Delcamp, J. H.; Gibson, E. A.; Meyer, G. J.; Pavone, M.; Pettersson, H.; Hagfeldt, A.; Freitag, M. Dye-Sensitized Solar Cells Strike Back. *Chem. Soc. Rev.* **2021**, *50*, 12450−12550.

(15) Brogdon, P.; Cheema, H.; Delcamp, J. H. Near-Infrared-Absorbing Metal-Free Organic, Porphyrin, and Phthalocyanine Sensitizers for Panchromatic Dye-Sensitized Solar Cells. *ChemSusChem* **2018**, *11*, 86−103.

(16) Mishra, A.; Fischer, M. K. R.; Bäuerle, P. Metal-Free Organic Dyes for Dye-Sensitized Solar Cells: From Structure: Property Relationships to Design Rules. *Angew. Chem., Int. Ed.* **2009**, *48*, 2474−2499.

(17) Liang, M.; Chen, J.; Plesse, C.; Beouch, L.; Aubert, P.-H.; Goubard, F.; Chevrot, C.; Sini, G.; Tian, H.; Yi, C. Y.; Nnazeeruddin, M. K.; Grätzel, M. Arylamine Organic Dyes for Dye-Sensitized Solar Cells. *Chem. Soc. Rev.* **2013**, *42*, 3453.

(18) Zhu, W.; Wu, Y.; Wang, S.; Li, W.; Li, X.; Chen, J.; Wang, Z.; Tian, H. Organic D-A-π-A Solar Cell Sensitizers with Improved Stability and Spectral Response. *Adv. Funct. Mater.* **2011**, *21*, 756−763.

(19) Aono, C. M.; Coutinho-Neto, M. D.; Miotto, R.; Homem-de-Mello, P. CAHM1: A Theory-Based Proposal for a New DSSC D−A−π−A Dye. *J. Phys. Chem. C* **2018**, *122*, 27256−27262.

(20) Wu, Y.; Zhu, W. Organic Sensitizers from D−π−A to D−A−π−A: Effect of the Internal Electron-Withdrawing Units on Molecular Absorption, Energy Levels and Photovoltaic Performances. *Chem. Soc. Rev.* **2013**, *42*, 2039−2058.

(21) Capodilupo, A. L.; de Marco, L.; Corrente, G. A.; Giannuzzi, R.; Fabiano, E.; Cardone, A.; Gigli, G.; Ciccarella, G. Synthesis and Characterization of a New Series of Dibenzofulvene Based Organic Dyes for DSSCs. *Dyes Pigm.* **2016**, *130*, 79−89.

(22) Jiang, X.; Marinado, T.; Gabrielsson, E.; Hagberg, D. P.; Sun, L.; Hagfeldt, A. Structural Modification of Organic Dyes for Efficient

Coadsorbent-Free Dye-Sensitized Solar Cells. *J. Phys. Chem. C* 2010, 114, 2799–2805.

(23) Hagberg, D. P.; Yum, J. H.; Lee, H. J.; de Angelis, F.; Marinado, T.; Karlsson, K. M.; Humphry-Baker, R.; Sun, L.; Hagfeldt, A.; Grätzel, M.; Nazeeruddin, M. K. Molecular Engineering of Organic Sensitizers for Dye-Sensitized Solar Cell Applications. *J. Am. Chem. Soc.* 2008, 130, 6259–6266.

(24) Haid, S.; Marszalek, M.; Mishra, A.; Wielopolski, M.; Teuscher, J.; Moser, J. E.; Humphry-Baker, R.; Zakeeruddin, S. M.; Grätzel, M.; Bäuerle, P. Significant Improvement of Dye-Sensitized Solar Cell Performance by Small Structural Modification in π-Conjugated Donor-Acceptor Dyes. *Adv. Funct. Mater.* 2012, 22, 1291–1302.

(25) Lin, L. Y.; Tsai, C. H.; Lin, F.; Huang, T. W.; Chou, S. H.; Wu, C. C.; Wong, K. T. 2,1,3-Benzothiadiazole-Containing Donor-Acceptor-Acceptor Dyes for Dye-Sensitized Solar Cells. *Tetrahedron* 2012, 68, 7509–7516.

(26) Lin, R. Y.-Y.; Lee, C.-P.; Chen, Y.-C.; Peng, J.-D.; Chu, T.-C.; Chou, H.-H.; Yang, H.-M.; Lin, J. T.; Ho, K.-C. Benzothiadiazole-Containing Donor−Acceptor−Acceptor Type Organic Sensitizers for Solar Cells with ZnO Photoanodes. *Chem. Commun.* 2012, 48, 12071–12073.

(27) Curiac, C.; Rodrigues, R. R.; Watson, J.; Hunt, L. A.; Devdass, A.; Jurss, J. W.; Hammer, N. I.; Fortenberry, R. C.; Delcamp, J. H. Iron Redox Shuttles with Wide Optical Gap Dyes for High-Voltage Dye-Sensitized Solar Cells. *ChemSusChem* 2021, 14, 3084–3096.

(28) Rodrigues, R. R.; Cheema, H.; Delcamp, J. H. A High-Voltage Molecular-Engineered Organic Sensitizer−Iron Redox Shuttle Pair: 1.4 V DSSC and 3.3 V SSM-DSSC Devices. *Angew. Chem., Int. Ed.* 2018, 57, 5472–5476.

(29) Zhang, L.; Yang, X.; Wang, W.; Gurzadyan, G. G.; Li, J.; Li, X.; An, J.; Yu, Z.; Wang, H.; Cai, B.; Hagfeldt, A.; Sun, L. 13.6% Efficient Organic Dye-Sensitized Solar Cells by Minimizing Energy Losses of the Excited State. *ACS Energy Lett.* 2019, 4, 943–951.

(30) Ji, J. M.; Zhou, H.; Eom, Y. K.; Kim, C. H.; Kim, H. K. 14.2% Efficiency Dye-Sensitized Solar Cells by Co-Sensitizing Novel Thieno[3,2-b]Indole-Based Organic Dyes with a Promising Porphyrin Sensitizer. *Adv. Energy Mater.* 2020, 10, No. 2000124.

(31) Zhang, D.; Stojanovic, M.; Ren, Y.; Cao, Y.; Eickemeyer, F. T.; Socie, E.; Vlachopoulos, N.; Moser, J. E.; Zakeeruddin, S. M.; Hagfeldt, A.; Grätzel, M. A Molecular Photosensitizer Achieves a Voc of 1.24 V Enabling Highly Efficient and Stable Dye-Sensitized Solar Cells with Copper(II/I)-Based Electrolyte. *Nat. Commun.* 2021, 12, No. 1777.

(32) Michaels, H.; Rinderle, M.; Freitag, R.; Benesperi, I.; Edvinsson, T.; Socher, R.; Gagliardi, A.; Freitag, M. Dye-Sensitized Solar Cells under Ambient Light Powering Machine Learning: Towards Autonomous Smart Sensors for the Internet of Things. *Chem. Sci.* 2020, 11, 2895–2906.

(33) Zeng, K.; Chen, Y.; Zhu, W.-H.; Tian, H.; Xie, Y. Efficient Solar Cells Based on Concerted Companion Dyes Containing Two Complementary Components: An Alternative Approach for Cosensitization. *J. Am. Chem. Soc.* 2020, 142, 5154–5161.

(34) Cui, Y.; Wu, Y.; Lu, X.; Zhang, X.; Zhou, G.; Miapeh, F. B.; Zhu, W.; Wang, Z.-S. Incorporating Benzotriazole Moiety to Construct D−A−π−A Organic Sensitizers for Solar Cells: Significant Enhancement of Open-Circuit Photovoltage with Long Alkyl Group. *Chem. Mater.* 2011, 23, 4394–4401.

(35) Ni, J.-S.; Yen, Y.-C.; Lin, J. T. Organic Dyes with a Fused Segment Comprising Benzotriazole and Thieno[3{,}2-b]Pyrrole Entities as the Conjugated Spacer for High Performance Dye-Sensitized Solar Cells. *Chem. Commun.* 2015, 51, 17080–17083.

(36) Liyanage, N. P.; Cheema, H.; Baumann, A. R.; Zylstra, A. R.; Delcamp, J. H. Effect of Donor Strength and Bulk on Thieno[3,4-b]-Pyrazine-Based Panchromatic Dyes in Dye-Sensitized Solar Cells. *ChemSusChem* 2017, 10, 2635–2641.

(37) Cheema, H.; Watson, J.; Peddapuram, A.; Delcamp, J. H. A 25 MA Cm−2 Dye-Sensitized Solar Cell Based on a near-Infrared-Absorbing Organic Dye and Application of the Device in SSM-DSCs. *Chem. Commun.* 2020, 56, 1741–1744.

(38) Jiang, M. L.; Wen, J. J.; Chen, Z. M.; Tsai, W. H.; Lin, T. C.; Chow, T. J.; Chang, Y. J. High-Performance Organic Dyes with Electron-Deficient Quinoxalinoid Heterocycles for Dye-Sensitized Solar Cells under One Sun and Indoor Light. *ChemSusChem* 2019, 12, 3654–3665.

(39) Pei, K.; Wu, Y.; Islam, A.; Zhang, Q.; Han, L.; Tian, H.; Zhu, W. Constructing High-Efficiency D−A−π−A-Featured Solar Cell Sensitizers: A Promising Building Block of 2,3-Diphenylquinoxaline for Antiaggregation and Photostability. *ACS Appl. Mater. Interfaces* 2013, 5, 4986–4995.

(40) Qu, S.; Wu, W.; Hua, J.; Kong, C.; Long, Y.; Tian, H. New Diketopyrrolopyrrole (DPP) Dyes for Efficient Dye-Sensitized Solar Cells. *J. Phys. Chem. C* 2010, 114, 1343–1349.

(41) Qu, S.; Qin, C.; Islam, A.; Wu, Y.; Zhu, W.; Hua, J.; Tian, H.; Han, L. A Novel D−A-π-A Organic Sensitizer Containing a Diketopyrrolopyrrole Unit with a Branched Alkyl Chain for Highly Efficient and Stable Dye-Sensitized Solar Cells. *Chem. Commun.* 2012, 48, 6972–6974.

(42) Higashino, T.; Kurumisawa, Y.; Nimura, S.; Iiyama, H.; Imahori, H. Enhanced Donor−π−Acceptor Character of a Porphyrin Dye Incorporating Naphthobisthiadiazole for Efficient Near-Infrared Light Absorption. *Eur. J. Org. Chem.* 2018, 2018, 2537–2547.

(43) Inoue, T.; Tsurui, M.; Yamagishi, H.; Nakazawa, Y.; Hamaguchi, N.; Watanabe, S.; Kitagawa, Y.; Hasegawa, Y.; Yamamoto, Y.; Tsuji, H. Long-Wavelength Visible to near Infrared Photoluminescence from Carbon-Bridged Styrylstilbene and Thiadiazole Conjugates in Organic and Aqueous Media. *RSC Adv.* 2021, 11, 6008–6013.

(44) Chatterjee, S.; Ie, Y.; Seo, T.; Moriyama, T.; Wetzelaer, G.-J. A. H.; Blom, P. W. M.; Aso, Y. Fluorinated Naphtho[1,2-c:5,6-c′]Bis[1,2,5]Thiadiazole-Containing π-Conjugated Compound: Synthesis, Properties, and Acceptor Applications in Organic Solar Cells. *NPG Asia Mater.* 2018, 10, 1016–1028.

(45) Wang, Y.; Michinobu, T. Benzothiadiazole and Its π-Extended, Heteroannulated Derivatives: Useful Acceptor Building Blocks for High-Performance Donor−Acceptor Polymers in Organic Electronics. *J. Mater. Chem. C* 2016, 4, 6200–6214.

(46) Frisch, M. J.; Trucks, G. W.; Schlegel, H. B.; Scuseria, G. E.; Robb, M. A.; Cheeseman, J. R.; Scalmani, G.; Barone, V.; Mennucci, B.; Petersson, G. A.et al.*Gaussian 09*, revision E.01; Gaussian, Inc.: Wallingford, CT 2013.

(47) Adamo, C.; Barone, V. Toward Reliable Density Functional Methods without Adjustable Parameters: The PBE0 Model. *J. Chem. Phys.* 1999, 110, 6158–6170.

(48) Chai, J.-D.; Head-Gordon, M. Long-Range Corrected Hybrid Density Functionals with Damped Atom−Atom Dispersion Corrections. *Phys. Chem. Chem. Phys.* 2008, 10, 6615.

(49) Yanai, T.; Tew, D. P.; Handy, N. C. A New Hybrid Exchange−Correlation Functional Using the Coulomb-Attenuating Method (CAM-B3LYP). *Chem. Phys. Lett.* 2004, 393, 51–57.

(50) Vijayan, S. M.; Sparks, N.; Roy, J.; Smith, C.; Tate, C.; Hammer, N.; Leszczynski, J.; Watkins, D. Evaluating Donor Effects in Isoindigo-Based Small Molecular Fluorophores. *J. Phys. Chem. A* 2020, 124, 10777–10786.

(51) Cossi, M.; Barone, V. Time-Dependent Density Functional Theory for Molecules in Liquid Solutions. *J. Chem. Phys.* 2001, 115, 4708.

(52) Nara, M.; Torii, H.; Tasumi, M. Correlation between the Vibrational Frequencies of the Carboxylate Group and the Types of Its Coordination to a Metal Ion: An Ab Initio Molecular Orbital Study. *J. Phys. Chem. A* 1996, 100, 19812–19817.

(53) Anselmi, C.; Mosconi, E.; Pastore, M.; Ronca, E.; De Angelis, F. Adsorption of Organic Dyes on TiO2 Surfaces in Dye-Sensitized Solar Cells: Interplay of Theory and Experiment. *Phys. Chem. Chem. Phys.* 2012, 14, 15963.

(54) Zheng, J.; Zhang, K.; Fang, Y.; Zuo, Y.; Duan, Y.; Zhuo, Z.; Chen, X.; Yang, W.; Lin, Y.; Wong, M. S.; Pan, F. How to Optimize the Interface between Photosensitizers and TiO2 Nanocrystals with

Molecular Engineering to Enhance Performances of Dye-Sensitized Solar Cells? *ACS Appl. Mater. Interfaces* **2015**, *7*, 25341−25351.

(55) Persson, P.; Gebhardt, J. C. M.; Lunell, S. The Smallest Possible Nanocrystals of Semiionic Oxides. *J. Phys. Chem. B* **2003**, *107*, 3336−3339.

(56) Pastore, M.; Fantacci, S.; de Angelis, F. Modeling Excited States and Alignment of Energy Levels in Dye-Sensitized Solar Cells: Successes, Failures, and Challenges. *J. Phys. Chem. C* **2013**, *117*, 3685−3700.

(57) Pastore, M.; Selloni, A.; Fantacci, S.; De Angelis, F. Electronic and Optical Properties of Dye-Sensitized TiO2 Interfaces. In *First Principles Approaches to Spectroscopic Properties of Complex Materials. Topics in Current Chemistry*; Di Valentin, C.; Botti, S.; C, M., Eds.; Springer: Berlin, Heidelberg, 2014.

(58) Paredes-Gil, K.; Mendizabal, F.; Páez-Hernández, D.; Arratia-Pérez, R. Electronic Structure and Optical Properties Calculation of Zn-Porphyrin with N-Annulated Perylene Adsorbed on TiO2 Model for Dye-Sensitized Solar Cell Applications: A DFT/TD-DFT Study. *Comput. Mater. Sci.* **2017**, *126*, 514−527.

(59) Li, P.; Cui, Y.; Song, C.; Zhang, H. A Systematic Study of Phenoxazine-Based Organic Sensitizers for Solar Cells. *Dyes Pigm.* **2017**, *137*, 12−23.

(60) Guo, M.; He, R.; Dai, Y.; Shen, W.; Li, M.; Zhu, C.; Lin, S. H. Electron-Deficient Pyrimidine Adopted in Porphyrin Sensitizers: A Theoretical Interpretation of π-Spacers Leading to Highly Efficient Photo-to-Electric Conversion Performances in Dye-Sensitized Solar Cells. *J. Phys. Chem. C* **2012**, *116*, 9166−9179.

(61) Lu, T.; Chen, F. Multiwfn: A Multifunctional Wavefunction Analyzer. *J. Comput. Chem.* **2012**, *33*, 580−592.

(62) Liu, Z.; Lu, T.; Chen, Q. An Sp-Hybridized All-Carboatomic Ring, Cyclo[18]Carbon: Electronic Structure, Electronic Spectrum, and Optical Nonlinearity. *Carbon* **2020**, *165*, 461−467.

(63) Reed, A. E.; Weinstock, R. B.; Weinhold, F. Natural Population Analysis. *J. Chem. Phys.* **1985**, *83*, 735−746.

(64) le Bahers, T.; Adamo, C.; Ciofini, I. A Qualitative Index of Spatial Extent in Charge-Transfer Excitations. *J. Chem. Theory Comput.* **2011**, *7*, 2498−2506.

(65) Meng, S.; Ren, J.; Kaxiras, E. Natural Dyes Adsorbed on TiO2 Nanowire for Photovoltaic Applications: Enhanced Light Absorption and Ultrafast Electron Injection. *Nano Lett.* **2008**, *8*, 3266−3272.

(66) Kakiage, K.; Aoyama, Y.; Yano, T.; Oya, K.; Kyomen, T.; Hanaya, M. Fabrication of a High-Performance Dye-Sensitized Solar Cell with 12.8% Conversion Efficiency Using Organic Silyl-Anchor Dyes. *Chem. Commun.* **2015**, *51*, 6315−6317.

(67) Anderson, A. Y.; Barnes, P. R. F.; Durrant, J. R.; O'Regan, B. C. Quantifying Regeneration in Dye-Sensitized Solar Cells. *J. Phys. Chem. C* **2011**, *115*, 2439−2447.

(68) Urbani, M.; Grätzel, M.; Khaja Nazeeruddin, M.; Torres, T. Meso-Substituted Porphyrins for Dye-Sensitized Solar Cells. *Chem. Rev.* **2014**, *114*, 12330−12396.

(69) Cole, J. M.; Pepe, G.; Al Bahri, O. K.; Cooper, C. B. Cosensitization in Dye-Sensitized Solar Cells. *Chem. Rev.* **2019**, *119*, 7279−7327.

(70) Dualeh, A.; de Angelis, F.; Fantacci, S.; Moehl, T.; Yi, C.; Kessler, F.; Baranoff, E.; Nazeeruddin, M. K.; Grätzel, M. Influence of Donor Groups of Organic D−π−A Dyes on Open-Circuit Voltage in Solid-State Dye-Sensitized Solar Cells. *J. Phys. Chem. C* **2012**, *116*, 1572−1578.

(71) Hardin, B. E.; Snaith, H. J.; McGehee, M. D. The Renaissance of Dye-Sensitized Solar Cells. *Nat. Photonics* **2012**, *6*, 162−169.

(72) Martin, R. L. Natural Transition Orbitals. *J. Chem. Phys.* **2003**, *118*, 4775−4777.

(73) Guido, C. A.; Cortona, P.; Mennucci, B.; Adamo, C. On the Metric of Charge Transfer Molecular Excitations: A Simple Chemical Descriptor. *J. Chem. Theory Comput.* **2013**, *9*, 3118−3126.

(74) Chaitanya, K.; Ju, X.-H.; Heron, B. M. Theoretical Study on the Light Harvesting Efficiency of Zinc Porphyrin Sensitizers for DSSCs. *RSC Adv.* **2014**, *4*, 26621−26634.

(75) Le Bahers, T.; Pauporté, T.; Scalmani, G.; Adamo, C.; Ciofini, I. A TD-DFT Investigation of Ground and Excited State Properties in Indoline Dyes Used for Dye-Sensitized Solar Cells. *Phys. Chem. Chem. Phys.* **2009**, *11*, 11276−11284.

(76) Cao, Y.; Liu, Y.; Zakeeruddin, S. M.; Hagfeldt, A.; Grätzel, M. Direct Contact of Selective Charge Extraction Layers Enables High-Efficiency Molecular Photovoltaics. *Joule* **2018**, *2*, 1108−1117.

(77) Chiu, C.-C.; Sheng, Y.-C.; Lin, W.-J.; Juwita, R.; Tan, C.-J.; Tsai, H.-H. G. Effects of Internal Electron-Withdrawing Moieties in D−A−π−A Organic Sensitizers on Photophysical Properties for DSSCs: A Computational Study. *ACS Omega* **2018**, *3*, 433−445.

(78) de Angelis, F.; Fantacci, S.; Mosconi, E.; Nazeeruddin, M. K.; Grätzel, M. Absorption Spectra and Excited State Energy Levels of the N719 Dye on TiO2 in Dye-Sensitized Solar Cell Models. *J. Phys. Chem. C* **2011**, *115*, 8825−8831.

(79) Yang, L.-N.; Sun, Z.-Z.; Chen, S.-L.; Li, Z.-S. The Effects of Various Anchoring Groups on Optical and Electronic Properties of Dyes in Dye-Sensitized Solar Cells. *Dyes Pigm.* **2013**, *99*, 29−35.

(80) Preat, J.; Michaux, C.; Jacquemin, D.; Perpète, E. A. Enhanced Efficiency of Organic Dye-Sensitized Solar Cells: Triphenylamine Derivatives. *J. Phys. Chem. C* **2009**, *113*, 16821−16833.

(81) Mendizabal, F.; Mera-Adasme, R.; Xu, W.-H.; Sundholm, D. Electronic and Optical Properties of Metalloporphyrins of Zinc on TiO2 Cluster in Dye-Sensitized Solar-Cells (DSSC). A Quantum Chemistry Study. *RSC Adv.* **2017**, *7*, 42677−42684.

(82) Ronca, E.; Pastore, M.; Belpassi, L.; Tarantelli, F.; de Angelis, F. Influence of the Dye Molecular Structure on the TiO2 Conduction Band in Dye-Sensitized Solar Cells: Disentangling Charge Transfer and Electrostatic Effects. *Energy Environ. Sci.* **2013**, *6*, 183−193.

(83) Li, G.; Wang, S.; Yang, S.; Liu, G.; Hao, P.; Zheng, Y.; Long, G.; Li, D.; Zhang, Y.; Yang, W.; Xu, L.; Gao, W.; Zhang, Q.; Cui, G.; Tang, B. Synthesis, Photophysical Properties and Two-Photon Absorption Study of Tetraazachrysene-Based N-Heteroacenes. *Chem. - Asian J.* **2019**, *14*, 1807−1813.

(84) Langis-Barsetti, S.; Maris, T.; Wuest, J. D. Synthesis of Salts of 1,2,5,6- and 1,4,5,8-Naphthalenetetramine. *ACS Omega* **2017**, *2*, 6023−6030.

(85) Li, Z.; Lu, J.; Tse, S. C.; Zhou, J.; Du, X.; Tao, Y.; Ding, J. Synthesis and Applications of Difluorobenzothiadiazole Based Conjugated Polymers for Organic Photovoltaics. *J. Mater. Chem.* **2011**, *21*, 3226−3233.

(86) Langis-Barsetti, S.; Maris, T.; Wuest, J. D. Molecular Organization of 2,1,3-Benzothiadiazoles in the Solid State. *J. Org. Chem.* **2017**, *82*, 5034−5045.

(87) Kawashima, K.; Miyazaki, E.; Shimawaki, M.; Inoue, Y.; Mori, H.; Takemura, N.; Osaka, I.; Takimiya, K. 5,10-Diborylated Naphtho[1,2-c:5,6-C′]Bis[1,2,5]Thiadiazole: A Ready-to-Use Precursor for the Synthesis of High-Performance Semiconducting Polymers. *Polym. Chem.* **2013**, *4*, 5224−5227.

(88) Lau, G. P. S.; Tsao, H. N.; Yi, C.; Zakeeruddin, S. M.; Grätzel, M.; Dyson, P. J. Enhancing the Stability of Porphyrin Dye-Sensitized Solar Cells by Manipulation of Electrolyte Additives. *ChemSusChem* **2015**, *8*, 255−259.